

The 2008 Eruption of Chaitén Volcano, Chile, as Viewed From ALOS, and the Importance of Complementary Satellite Looks

by Charles Wicks, United States Geological Survey

A rare explosive rhyolite eruption occurred on 2 May 2008 at Chaitén Volcano in Chile, a type of eruption that had not been seen since the 1912 eruption of Novarupta in Alaska. Chaitén had not erupted for thousands of years before the 2008 eruption and it was not monitored prior to the eruption. The eruption occurred with only 2 days of detected precursory activity and the nearly crystal-free rhyolitic magma has been shown to have migrated from greater than 5-km depth to the surface in less than about 4 hours (Castro and Dingwell, 2009). Although Chaitén was not part of an ongoing ground-based monitoring network, it was a part of the Japan Aerospace Exploration Agency's (JAXA) ongoing mission for Advanced Land Observing Satellite-Phased Array L-band Synthetic Aperture Radar (ALOS-PALSAR) data acquisition. These data have enabled modeling of the deformation related to this rare rhyolite eruption. From this model, one can infer that the magma reached the surface quickly via diking, local faults controlled the emplacement of a rhyolite reservoir beneath Chaitén, and the source of the magma is probably beneath Michimahuida Volcano approximately 15-km east of Chaitén (Figure 1).

Although the study area is heavily vegetated, the approximately 2-year ascending- and descending-mode interferograms (Figure 1) that span the eruption, and subsequent rhyolite dome emplacement, clearly show the related surface deformation. The descending-mode interferogram displays a broad area of movement away from the satellite that encompasses the entire Michimahuida-Chaitén volcanic complex, but the deforming area is restricted to a small area west of Chaitén in the ascending-mode interferogram. The radar beams from both modes intersect the Earth's surface at an angle of about 39° from vertical. Consideration of the radar geometry, shown schematically in Figure 1c, shows the main deformation source responsible for the broad-deformation signal should be a sill-like collapsing body that dips to the

East-Northeast with a dip angle that is nearly complementary to the radar-incidence angle in the ascending geometry. Modeling of the interferograms favors a three-body deformation source (Figure 2): 1) a deep dipping, sill-like body (approximately 10 km beneath Chaitén) that we interpret to be a reservoir of rhyolitic magma, 2) an inflated dike that reaches from the rhyolite reservoir to the surface at Chaitén, and 3) a shallow lath-like collapsing conduit that extends vertically from the rhyolite reservoir to Chaitén.

Although the ascending ALOS-PALSAR data were available soon after the eruption, it was not until the descending data was acquired by JAXA in 2010 that the picture of deformation became complete. Before descending data were available over Chaitén, the model that best fit the ascending ALOS data (Figure 1a) was a narrow, steeply dipping, collapsing rectangular dike (also in Fournier, et al., 2010), similar to the lath-like

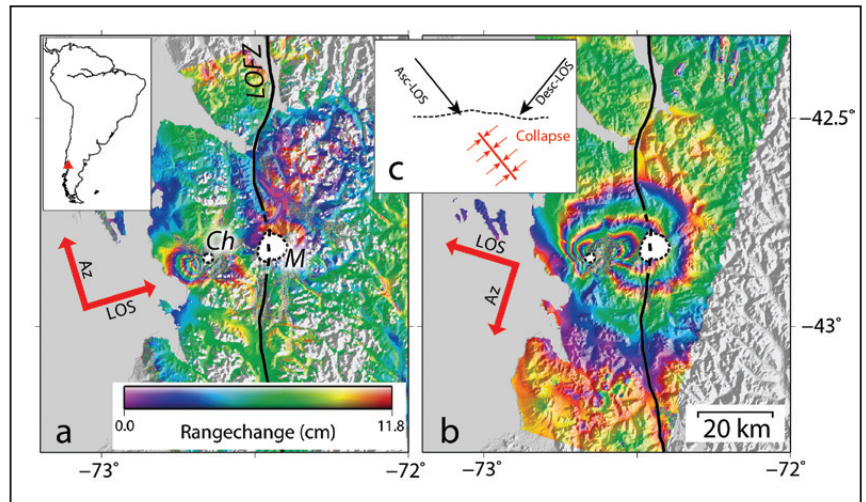


Figure 1: Index map and examples of two, approximately, 2-year interferograms spanning the Chaitén eruption. The red triangle in the inset map shows the location of Chaitén Volcano. **a)** An ascending interferogram. The black line labeled LOFZ shows the location of the main strand of the Liquiñe-Ofqui fault zone. The colorscale maps the colors into changes in range distance between the satellite and the ground. The dashed, white-filled circular area labeled Ch is Chaitén Caldera. The larger dashed, white-filled area labeled M is the approximate outline of Michimahuida Caldera. The red arrow labeled Az shows the flight direction of the ALOS satellite. The red arrow labeled LOS shows the look direction from the satellite to the ground. **b)** A descending interferogram. **c)** Schematic diagram showing geometry of the collapsing body relative to satellite geometry.

Continued from front page

conduit part of the model in Figure 2. Since nearly one km³ of material was erupted, more surface deformation than can be seen in the ascending interferogram (Figure 1a) was expected, and indeed the descending-mode interferogram (Figure 1b) shows a much different deformation field that is more appropriate to the size of the eruption. This study shows the deformation

source related to an eruption and, thus the inferred-magmatic system can be complex and illustrates the need for multiple, complementary satellite looks to study volcano deformation in future SAR-satellite missions. For more information about this study, see Wicks, et al., 2011 (http://volcanoes.usgs.gov/activity/methods/insar/research_results.php).

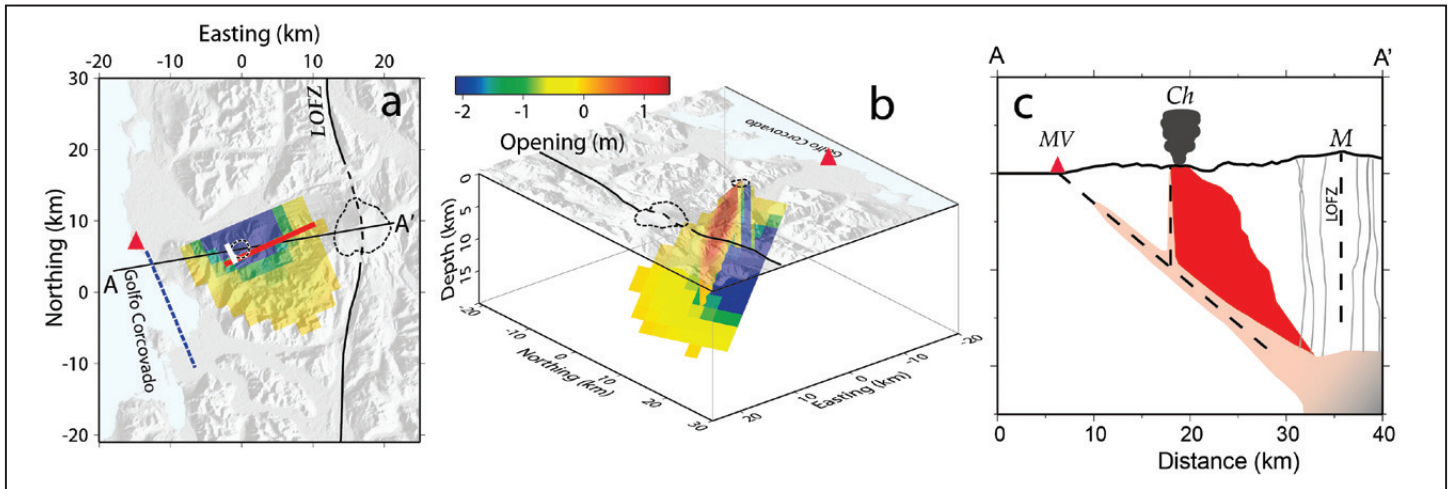


Figure 2: Three deformation sources found by modeling the interferograms in Figure 1. The red triangle in each panel shows the location of Morro Vilcún, an undated rhyolite plug. **a)** Map view of the deformation sources. The bold red line is the surface trace of the dike, the short bold white line (on the west side of Chaitén) is the surface trace of the lath-like conduit, and the blue-dashed line shows where the modeled plane containing the rhyolite reservoir intersects the surface. The location of cross-section A-A' in Figure 2c is shown with the East-Northeast trending black line. **b)** A 3-D perspective of the deformation sources viewed from the Northeast. **c)** A schematic cross-section through A-A' showing the location of the three deformation sources (the dike is red) and Michimahuida Volcano (M), Chaitén Volcano (Ch), and Morro Vilcún.

Integrating ALOS PALSAR into the Forest Service Vegetation Classification and Mapping Process

by Abigail Schaaf, USDA Forest Service, Don Atwood, Alaska Satellite Facility, and Mark Riley, USDA Forest Service

Passive optical, remotely-sensed imagery has a long and successful history as a key data layer for the USDA Forest Service vegetation image classification and mapping process. With the capability to penetrate cloud and fog, active SAR is not bound by the same physical and temporal restrictions as passive optical sensors.

In cooperation with ASF, the Forest Service evaluated the integration of ALOS-PALSAR data into the existing vegetation mapping process for a current project on the Copper River Delta (CRD) region in the Chugach National Forest in Alaska (Figure 3). The project area consists of a portion of the CRD, with a total of 552,356 acres used for the analysis. One of the strengths of the PALSAR data is the medium-resolution cell size, which promotes a more exhaustive comparison to passive optical datasets.

The Forest Service employs the advanced R-based ensemble classifier Random Forest to statistically extract the most accurate information possible from robust image-based geospatial datasets

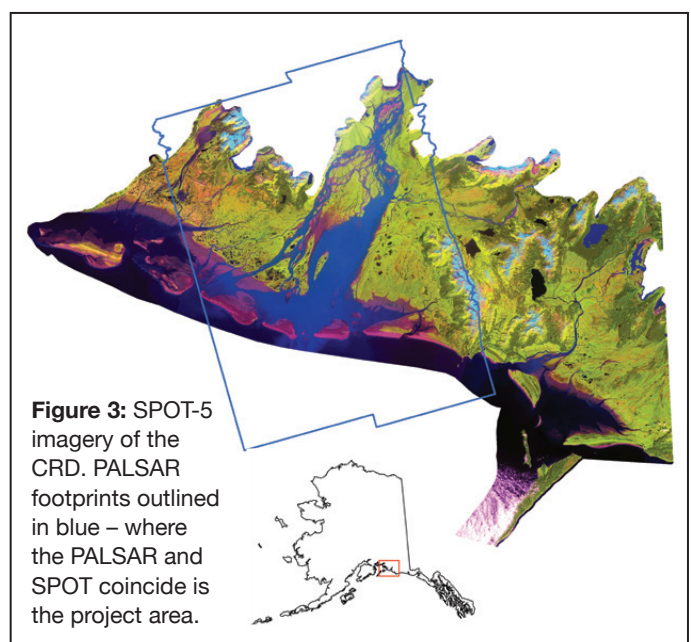


Figure 3: SPOT-5 imagery of the CRD. PALSAR footprints outlined in blue - where the PALSAR and SPOT coincide is the project area.

and known-field data points. For this study, existing vegetation map types were characterized by dominance cover type and basic lifeform cover type, and were classified at the stand level, using multiple combinations of the input data layers. Following the classification process, an evaluation of the contribution of the PALSAR data was conducted.

In addition to the PALSAR data, the project used SPOT-5 multispectral satellite imagery and a 20-meter SPOT High-Resolution Stereo (HRS) Digital Surface Model (DSM). Image derivatives, indices, and other dataset transformations provided additional data-mining inputs. The two quad-polar PALSAR scenes used for this study were acquired on May 27 and July 12, 2009, a near concurrent collection with the multispectral SPOT-5 data. Both scenes had a range and azimuth pixel size of 10 meters and were processed to Level 1.1. After the polarimetry data layers were generated, they were resampled from 10 meters to 5 meters, using ArcMap's Resample Tool and Bilinear Interpolation as the resampling technique to match the spatial resolution of the SPOT-5 imagery and digital-elevation model (DEM) data.

Established techniques for pre-processing of SAR data were essential to the successful extraction of physical properties. Polarimetric processing was performed using two free, open-source tools provided by the European Space Agency (PolSARpro) and ASF (MapReady Remote Sensing Toolkit). These software tools enabled the derivation of PALSAR-polarimetry layers that accurately expressed the scattering matrix of surface feature objects.

To evaluate the contribution of the PALSAR information, the mapping was performed using three combinations of input predictor layers: 1) standalone PALSAR data layers; 2) a combination of PALSAR data layers, SPOT 5, and DSM data; 3) only the SPOT and DSM data. For each combination of predictor layers, a Random Forest classification was performed to three hierarchical cover type levels: 1) vegetation dominance; 2) vegetation sub-cover; 3) vegetation lifeform. Image-classification training data, essential to the data-mining process, was collected in the field and from high-resolution digital-orthorectified aerial photography.

It was found that the integration of the PALSAR data in the vegetation mapping and classification process provides an improvement to the accuracy of the classification results as shown in the table. Percent-error calculations used Kappa statistics and errors of omission and commission.

Input Data Layer(s)	Classification scheme	% Error
PALSAR polarimetry	Lifeform Cover Type	27.85
SPOT, DEM	Lifeform Cover Type	17.71
PALSAR, SPOT, DEM	Lifeform Cover Type	15.82
PALSAR polarimetry	Sub-Cover Type	49.05
SPOT, DEM	Sub-Cover Type	34.06
PALSAR, SPOT, DEM	Sub-Cover Type	30.06
PALSAR polarimetry	Dominance Cover Type	59.81
SPOT, DEM	Dominance Cover Type	45.53
PALSAR, SPOT, DEM	Dominance Cover Type	43.67

With fewer classes and less spectral variability, the lifeform cover type had the least classification error. This level of classification is the broadest of the three and affords the least amount of detail, and does not differentiate vegetation-species type. Figure 4 illustrates the mapped-classification results at the lifeform level.

Figure 4a represents the SPOT, DSM, and PALSAR classification result. Figure 4b represents the SPOT and DSM classification result and 4c represents the classification results from the PALSAR data alone. Visually, there is very little difference between the classification results of 4a and 4b. Figure 4c, the PALSAR data alone, is significantly different from the other combinations that included the SPOT and DSM data. The results in 4c indicate there is more water, less sparsely

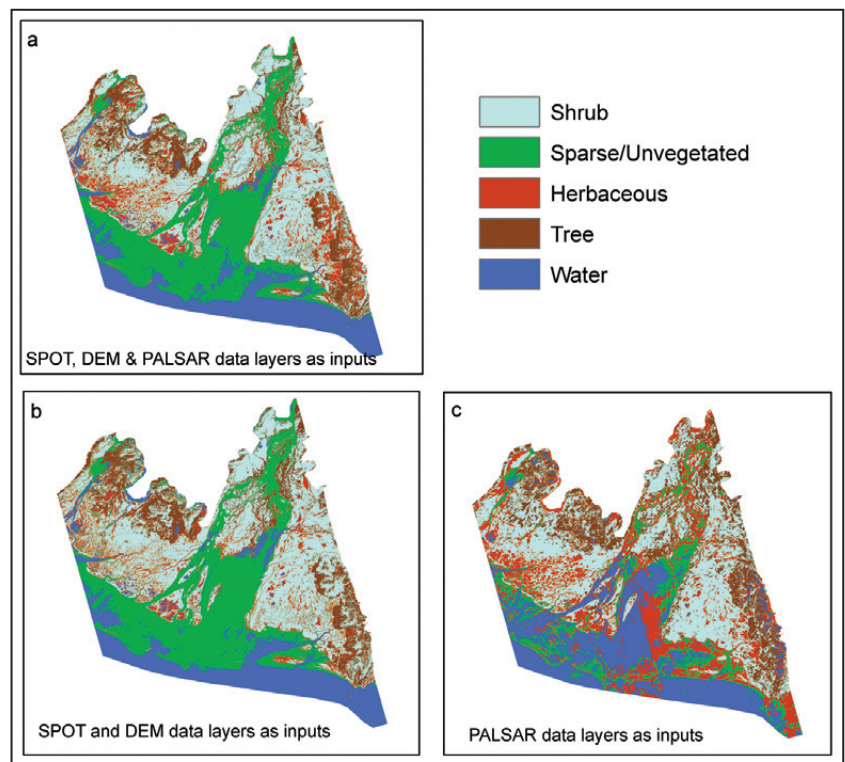


Figure 4: Random Forest classification results at the lifeform level.



Alaska Satellite Facility
UAF Geophysical Institute
903 Koyukuk Drive
PO Box 757320
Fairbanks, AK 99775-7320

www.asf.alaska.edu

Continued from page 3

vegetated/unvegetated and shrub, and more forest in comparison to 4a and 4b. It was found that the sparsely vegetated, unvegetated, and water classes were very mixed when only the PALSAR data layers were used as inputs. Figure 4 demonstrates that the PALSAR data does less to drive the classification than the optical and topographic data. It is clear that when included in the classification with the SPOT and DSM data, the PALSAR data enhances, but does not control the results.

While the inclusion of PALSAR into the classification process resulted in only a marginal-statistical increase in accuracy, it is across the whole project area where this increase in accuracy is positively aggregated. While a classification-accuracy improvement of only a few percent may seem statistically insignificant, this should be measured in terms of additional accuracy across an entire project area, that could add up to several-thousand hectares.

For future research and analysis, evaluating each of the SAR-polarimetry datasets, independently and with auxiliary data layers, may determine which are performing better than others. Additionally, it may be beneficial to use the SAR data in generating the image segments, as opposed to only the optical data, including the radar imagery, may improve species-level delineations.

Submissions and Subscriptions



This newsletter, published by ASF, was created to provide detailed information about special projects and noteworthy developments, as well as science articles highlighting the use of ASF data.

To receive the newsletter by postal mail, please fill out the subscription form linked to the ASF home page at www.asf.alaska.edu. Current and back issues of the newsletter can also be obtained through the ASF Web site.

Submissions to the *ASF News & Notes* and suggestions about content are always welcome. If you are interested in contributing materials, please call or send an e-mail to the editor:

Vicky Wolf, ASF User Support

907-474-6166 | uso@sf.alaska.edu

Alaska Satellite Facility's Management

Nettie La Belle-Hamer, *ASF Director*

Scott Arko, *ASF Deputy Director*